Universität Regensburg
Mathematik

Solving the Cahn-Hilliard variational inequality with a semi-smooth Newton method

Luise Blank, Martin Butz and Harald Garcke

Preprint Nr. 07/2009

Solving the Cahn-Hilliard variational inequality with a semi-smooth Newton method

Luise Blank, Martin Butz, Harald Garcke,
Version vom March 26, 2009

Abstract

The Cahn-Hilliard variational inequality is a non-standard parabolic variational inequality of fourth order for which straightforward numerical approaches cannot be applied. We propose a primal-dual active set method which can be interpreted as a semi-smooth Newton method as solution technique for the discretized Cahn-Hilliard variational inequality. A (semi-)implicit Euler discretization is used in time and a piecewise linear finite element discretization of splitting type is used in space leading to a discrete variational inequality of saddle point type in each time step. In each iteration of the primal-dual active set method a linearized system resulting from the discretization of two coupled elliptic equations which are defined on different sets has to be solved. We show local superlinear convergence of the primal-dual active set method and demonstrate its efficiency with several numerical simulations.

Key Words: Cahn-Hilliard equation, active-set methods, semi-smooth Newton methods, gradient flows, PDE-constraint optimization, saddle point structure.

AMS subject classification: 35K55, 35K85, 90C33, 49N90, 80A22, 82C26, 65M60

1 Introduction

The Cahn-Hilliard equation was initially introduced to model phase separation in binary alloys [10]. By now the Cahn-Hilliard equation has found many applications ranging from classical aspects in materials science [30, 21] over image processing [16], fluid dynamics [29], topology optimization [37] up to the modelling of mineral growth [27] and galaxy structure formation [33]. The Cahn-Hilliard equation can model interface motion in so called conserved systems, i.e. in systems where the concentration of a species or the volume occupied by a phase is conserved. In these applications Cahn-Hilliard variational inequalities are frequently used.

In this paper we propose a numerical method for solving Cahn-Hilliard variational inequalities and we heavily use the gradient flow structure of the Cahn-Hilliard model. We interpret the time discretized version of the gradient flow as a PDE-constraint optimization problem where in addition pointwise inequality constraints have to hold. The PDE-constraint minimization problem which we obtain is

non-standard as the objective functional obtains L^2-norm of gradients rather than the L^2-norms of the involved functions itself. We propose to solve the fully discretized system with a primal-dual active set method which can be reinterpreted as a semi-smooth Newton method. It turns out that this approach is superior to earlier numerical methods for Cahn-Hilliard variational inequalities. Its efficiency in each iteration step is comparable to a method proposed by Gräser and Kornhuber [22]. They introduce and analyse a Uzawa-multigrid algorithm. There in each iteration step an intermediate primal-active set is determined with the help of obstacle problems which are solved with a monotone multigrid method. In a second step a linear subproblem similar to ours where only the right hand side differs has to be solved, to then update the chemical potential by a damped gradient-type method. After convergence the phase field is determined. In contrast we determine the active sets in a simple way using approximations of the primal and dual variables, we have to solve the same linear subproblem where we solve for the chemical potential and the phase field simultaneously. Banas and Nürnberg [2] extended the idea of [22] and apply a monotone multigrid approach to the whole system of Cahn-Hilliard inequalities. Computational comparisons are not available up to now.

The outline of the paper is as follows. In the remainder of this section we introduce the Cahn-Hilliard variational inequality. We will interpret the implicit time discretization of the Cahn-Hilliard variational inequality as a PDE-constraint optimization problem in Section 2. In Section 3 we introduce a primal-dual active set approach for the time discretized Cahn-Hilliard variational inequality and we formulate a finite element method for a splitting formulation of the Cahn-Hilliard variational inequality in Section 4. We also show local superlinear convergence. Finally, we numerically analyse the behaviour of the method with the help of four examples of different type and show some simulations in Section 5.

Since the gradient flow perspective is important for what follows we choose to derive the Cahn-Hilliard equations as a gradient flow. We remark that our derivation will be formal. We now consider a vector space $\mathbf{Z}$ and an affine subspace $\mathbf{U} \subset \mathbf{Z}$, i.e. there exists a $\overline{u} \in \mathbf{Z}$ and a linear space $\mathbf{Y} \subset \mathbf{Z}$ such that $\mathbf{U} = \overline{u} + \mathbf{Y}$. The gradient of a sufficiently smooth function $E : \mathbf{U} \to \mathbb{R}$ depends on the inner product chosen for $\mathbf{Z}$. We define the first variation of E at a point $u \in \mathbf{U}$ in a direction $v \in \mathbf{Y}$ by

$$\frac{\delta E}{\delta u}(u)(v) := \lim_{\delta \to 0} \frac{E(u + \delta v) - E(u)}{\delta} .$$

We say $\operatorname{grad}_{\mathbf{Z}} E(u) \in \mathbf{Z}$ is a gradient of E with respect to the inner product $(.,.)_{\mathbf{Z}}$ on $\mathbf{Z}$ if

$$(\operatorname{grad}_{\mathbf{Z}} E(u), v)_{\mathbf{Z}} = \frac{\delta E}{\delta u}(u)(v) \quad \text{for all} \quad v \in \mathbf{Y} .$$

Now the gradient flow of E with respect to the inner product $(.,.)_{\mathbf{Z}}$ is given as

$$\partial_t u(t) = -\operatorname{grad}_{\mathbf{Z}} E(u(t)) . \tag{1}$$

The energy decreases in time due to the inequality

$$\frac{d}{dt}E(u(t)) = (\mathrm{grad}_{\mathbf{Z}}E(u(t)), \partial_t u(t))_{\mathbf{Z}} = -\|\partial_t u\|^2_{\mathbf{Z}} \leq 0.$$

In the following, in order to derive the Cahn-Hilliard equation, we introduce the Ginzburg-Landau energy $E : H^1(\Omega) \to \mathbb{R}$ as

$$E(u) = \int_\Omega \{\tfrac{\gamma\varepsilon}{2}|\nabla u|^2 + \tfrac{1}{\varepsilon}\psi(u)\}dx \tag{2}$$

where $\Omega \subset \mathbb{R}^d$ is a bounded domain with Lipschitz boundary, $\gamma > 0$ is a constant related to the interfacial energy density and ψ is a double well potential, e.g. $\psi(u) = (1-u^2)^2$ or an obstacle potential, e.g.

$$\psi(u) = \left\{ \begin{array}{ll} \psi_0(u) & u \in [-1,1] \\ \infty & \text{elsewhere} \end{array} \right\} = \psi_0(u) + I_{[-1,1]}(u) \tag{3}$$

where ψ_0 is smooth and $I_{[-1,1]}$ is the indicator function, i.e. $I_{[-1,1]}$ is set to infinity outside the interval $[-1,1]$ and to 0 on $[-1,1]$. In the following we will choose

$$\psi_0(u) = \tfrac{1}{2}(1-u^2) \tag{4}$$

which is the typical choice in the literature, see e.g. [7], but other non-convex functions are possible. In the Cahn-Hilliard model different phases correspond to the values $u = \pm 1$. On an interface a solution rapidly changes from values close to 1 to values close to -1 and the thickness of this interfacial region is proportional to the parameter ε in (2), see e.g. Figure 1.

If ψ is smooth the first variation of E in a direction v is given as

$$\frac{\delta E}{\delta u}(u)(v) = \int_\Omega (\gamma\varepsilon\nabla u \cdot \nabla v + \tfrac{1}{\varepsilon}\psi'(u)v)\,. \tag{5}$$

Choosing $\mathbf{Z} = L^2(\Omega)$, $\mathbf{U} = \mathbf{Y} = H^1(\Omega)$ and $\overline{u} = 0$ we obtain

$$\mathrm{grad}_{L^2}E(u) = -\gamma\varepsilon\Delta u + \tfrac{1}{\varepsilon}\psi'(u) \tag{6}$$

and the resulting gradient flow equation gives the so called Allen-Cahn equation. We remark here that for (6) we also need to require $\frac{\partial u}{\partial n} = 0$ on $\partial\Omega$ where n is the outer unit normal to $\partial\Omega$.

As mentioned above in the Cahn-Hilliard model the total concentration, i.e. $\int_\Omega u(x)dx$ is assumed to be conserved. Denoting by $\fint_\Omega u$ the mean value of a function u, we now define for a given $m \in (-1,1)$ the sets

$$\mathbf{U} := \{u \in H^1(\Omega) \mid \fint_\Omega u = m\}\,, \quad \mathbf{Y} := \{u \in H^1(\Omega) \mid \fint_\Omega u = 0\}.$$

In addition we introduce $\mathbf{Z} = H^{-1}(\Omega) = \{u' \in (H^1(\Omega))' \mid \langle u', 1\rangle = 0\}$, i.e. all bounded linear functionals on $H^1(\Omega)$ that vanish on constant functions. Here and in what follows $\langle ., . \rangle$ denotes the dual pairing. On $\mathbf{Z} = H^{-1}(\Omega)$ we define the H^{-1}-inner product for $v_1, v_2 \in \mathbf{Z}$ as

$$(v_1, v_2)_{H^{-1}} := \int_\Omega \nabla(-\Delta)^{-1} v_1 \cdot \nabla(-\Delta)^{-1} v_2 \tag{7}$$

where $y = (-\Delta)^{-1} v$ is the weak solution of $-\Delta y = v$, $\frac{\partial y}{\partial n} = 0$. We remark that the solution to this elliptic problem is only defined up to a constant and we always choose y such that $\fint_\Omega y = 0$. The function space $\mathbf{Y}$ is canonically embedded into $\mathbf{Z}$ since $u \in \mathbf{Y}$ can be related to the linear functional $y \mapsto \int_\Omega uy$. For $v_1, v_2 \in \mathbf{Y}$ we obtain

$$(v_1, v_2)_{H^{-1}} = (v_1, (-\Delta)^{-1} v_2)_{L^2} = ((-\Delta)^{-1} v_1, v_2)_{L^2} .$$

These identities also hold more generally for functions $v_1, v_2 \in L^2(\Omega)$ with mean value zero. To compute the H^{-1}-gradient of E we now need to find $\mathrm{grad}_{H^{-1}} E(u) \in \mathbf{Z}$ such that

$$(v, \mathrm{grad}_{H^{-1}} E(u))_{H^{-1}} = \frac{\delta E}{\delta u}(u)(v) \text{ holds for all } v \in \mathbf{Y}.$$

From the above we obtain $(v, (-\Delta)^{-1} \mathrm{grad}_{H^{-1}} E(u))_{L^2} = (v, \mathrm{grad}_{L^2} E(u))_{L^2}$ and hence

$$\mathrm{grad}_{H^{-1}} E(u) = (-\Delta) \mathrm{grad}_{L^2} E(u) . \tag{8}$$

Then, the Cahn-Hilliard equation is given as the H^{-1}-gradient flow of the Ginzburg–Landau energy E. If ψ is smooth we obtain the fourth order parabolic equation

$$\partial_t u = -\mathrm{grad}_{H^{-1}} E(u) = \Delta \left(-\gamma\varepsilon \Delta u + \tfrac{1}{\varepsilon} \psi'(u) \right) \tag{9}$$

or equivalently introducing the so called chemical potential w the equation can be rewritten as a system as follows

$$\partial_t u = \Delta w , \tag{10}$$

$$w = -\gamma\varepsilon \Delta u + \tfrac{1}{\varepsilon} \psi'(u). \tag{11}$$

In addition the boundary conditions $\frac{\partial u}{\partial n} = \frac{\partial w}{\partial n} = 0$ on $\partial\Omega$ have to hold. Let us remark, that in this formulation we do not necessarily have $\fint_\Omega w = 0$, i.e. in general $w \neq -(-\Delta)^{-1} \partial_t u$ but both functions only differ by an additive constant.

It is also possible to derive the Cahn-Hilliard equation from the mass balance law and in this case $-\nabla w$ is the mass flux where for simplicity a mobility coefficient was taken to be one, see e.g. Elliott [18] or Novick-Cohen [30].

The presentation so far is appropriate for smooth functions ψ. If the energy has the double obstacle form (3) we differentiate $I_{[-1,1]}$ in the sense of subdifferentials,

i.e. for a $u \in L^2(\Omega)$ with $|u| \leq 1$ we obtain that $\mu \in L^2(\Omega)$ is in the subdifferential of $I_{[-1,1]}$ at u if and only if

$$\mu \in \partial I_{[-1,1]}(u) = \begin{cases} (-\infty, 0] & \text{if } u = -1\,, \\ 0 & \text{for } u \in (-1,1)\,, \\ [0, \infty) & \text{if } u = 1\,, \end{cases} \tag{12}$$

is fulfilled pointwise almost everywhere. This can be rewritten in the following complementarity form

$$\mu = \mu_+ - \mu_-,\ \mu_+ \geq 0, \mu_- \geq 0,\ \mu_+(u-1) = 0,\ \mu_-(u+1) = 0 \tag{13}$$

which also has to hold almost everywhere. In this case the H^{-1}-gradient flow has the form

$$\partial_t u = \Delta w\,, \tag{14}$$

$$w = -\gamma\varepsilon\Delta u + \tfrac{1}{\varepsilon}(\psi_0'(u) + \mu) \tag{15}$$

with $\mu \in \partial I_{[-1,1]}(u)$, $|u| \leq 1$ and zero Neumann boundary conditions for u and w. This formulation can be restated in a variational inequality formulation, see e.g. Blowey and Elliott [7] or Kinderlehrer and Stampacchia [26] and Friedman [20] for other obstacle problems, as follows:

$$\partial_t u = \Delta w\,, \tag{16}$$

$$(w, \xi - u)_{L^2} \leq \gamma\varepsilon(\nabla u, \nabla(\xi - u))_{L^2} + \tfrac{1}{\varepsilon}(\psi_0'(u), \xi - u)_{L^2} \quad \forall\ \xi \in H^1(\Omega), |\xi| \leq 1\,, \tag{17}$$

together with $|u| \leq 1$ a.e.. For this formulation it can be shown that a unique solution u exists which is H^2-regular in space. More precisely the following theorem, see [7], is true.

Theorem 1.1 *Assume Ω is convex or $\partial\Omega \in C^{1,1}$, $u_0 \in H^1(\Omega)$ with $|u_0| \leq 1$ and $\fint_\Omega u_0 = m \in (-1,1)$. Then there exists a unique pair (u, w) such that*

$$u \in H^1(0,T; (H^1(\Omega))') \cap L^2(0,T; H^2(\Omega)) \cap L^\infty(0,T; H^1(\Omega))\,,$$

$|u| \leq 1$ a.e. and $w \in L^2(0,T; H^1(\Omega))$ which solves

$$\langle \partial_t u, \eta \rangle + (\nabla w, \nabla \eta)_{L^2} = 0 \quad \text{for all } \eta \in H^1(\Omega) \quad \text{and } t \in (0,T) \qquad \text{a.e.}$$

together with the variational inequality (17) and $u(0,\cdot) = u_0$.

In particular $\mu = \varepsilon w + \gamma\varepsilon^2\Delta u - \psi_0'(u) \in L^2(\Omega_T)$.

2 Cahn-Hilliard variational inequalities and PDE-constraint optimization

Given discrete times $t_n = n\tau, n \in \mathbb{N}_0$, where $\tau > 0$ is a given time step the backward Euler discretization of the gradient flow equation (1) is given as

$$\tfrac{1}{\tau}(u^n - u^{n-1}) = -\mathrm{grad}_{H^{-1}} E(u^n)\,. \tag{18}$$

This time discretization has a natural variational structure. In fact one can compute u^n as the solution of the minimization problem

$$\min_{u\in\mathbf{U}}\{E(u) + \tfrac{1}{2\tau}\|u - u^{n-1}\|^2_{H^{-1}}\}\,. \tag{19}$$

One hence tries to decrease the energy E but has to take into account that deviations from the solution at the old time step costs where the cost depends on the norm on $\mathbf{Z} = H^{-1}(\Omega)$. As Euler-Lagrange equation for (19) we obtain the backward Euler discretization (18). We remark here that (18) might have solutions which are not necessarily global minimizers of the minimization problem (19). In the case of the Cahn-Hilliard model we need to minimize

$$\int_\Omega \left\{\tfrac{\gamma\varepsilon}{2}|\nabla u|^2 + \tfrac{1}{\varepsilon}\psi(u)\right\} dx + \tfrac{1}{2\tau}\|u - u^{n-1}\|^2_{H^{-1}} \tag{20}$$

under all $u \in H^1(\Omega)$ with $\fint_\Omega u = \fint_\Omega u^{n-1} = m$. In order to compute the H^{-1}-norm of $u - u^{n-1}$ we need to solve a Poisson problem and hence we obtain, in the case of the obstacle potential, the following PDE-constraint optimization problem

$$\min \left\{ \tfrac{\gamma\varepsilon}{2}\int_\Omega |\nabla u|^2 + \tfrac{1}{\varepsilon}\int_\Omega \psi_0(u) + \tfrac{\tau}{2}\int_\Omega |\nabla v|^2 \right\} \tag{21}$$

$$\text{such that} \quad \tau\Delta v = u - u^{n-1}\,, \tag{22}$$

$$|u| \le 1,\ \fint_\Omega u = m\,,$$

$$\text{with } \tfrac{\partial v}{\partial n} = 0 \text{ on } \partial\Omega \text{ and } \fint_\Omega v = 0.$$

This formulation has the form of an optimal control problem where u is the control and v is the state.

We now introduce Lagrange multipliers $w \in H^1(\Omega)$ for the weak formulation of (22), and $\kappa \in \mathbb{R}$ for $\fint_\Omega v = 0$ and define the Lagrangian

$$\mathcal{L}(u, v, w, \lambda) := \tfrac{\gamma\varepsilon}{2}\int_\Omega |\nabla u|^2 + \tfrac{1}{\varepsilon}\int_\Omega \psi_0(u) + \tfrac{\tau}{2}\int_\Omega |\nabla v|^2 - \int_\Omega \tau\nabla w\cdot\nabla v - \int_\Omega (u - u^{n-1})w + \kappa\fint_\Omega v\,.$$

With this Lagrangian the equality constraints are incorporated. In fact the equality constraints are obtained as the first variation of $\mathcal{L}$ with respect to w and κ. In

particular, we obtain $\fint_\Omega u = \fint_\Omega u^{n-1} = m$ if we vary w by a constant. This implies that w acts as a Lagrange multiplier simultaneously for the equality constraints (22) and $\fint_\Omega u = m := \fint_\Omega u^{n-1}$.

Introducing appropriately scaled Lagrange multipliers μ, namely with $\frac{1}{\varepsilon}$, for the pointwise box-constraints we obtain the following version of the KKT-system where (23), (25) and (26) have to be understood in its weak form.

$$\begin{aligned}
\tau\Delta(w-v) &= \kappa \text{ in } \Omega,\ \frac{\partial w}{\partial n} = \frac{\partial v}{\partial n} \text{ on } \partial\Omega\,, && (23)\\
\fint_\Omega v &= 0\,,\ \kappa = 0\,, && (24)\\
\tfrac{1}{\tau}(u-u^{n-1}) &= \Delta v \text{ in } \Omega,\ \frac{\partial v}{\partial n} = 0 \text{ on } \partial\Omega\,, && (25)\\
w + \gamma\varepsilon\Delta u - \tfrac{1}{\varepsilon}\psi_0'(u) - \tfrac{1}{\varepsilon}\mu &= 0 \text{ in } \Omega,\ \frac{\partial u}{\partial n} = 0 \text{ on } \partial\Omega\,, && (26)\\
\mu &= \mu_+ - \mu_-,\ \mu_+ \geq 0, \quad \mu_- \geq 0,\ \text{a.e. in } \Omega\,, && (27)\\
\mu_+(u-1) &= 0,\ \mu_-(u+1) = 0,\ \text{a.e. in } \Omega\,, && (28)\\
\text{and} \qquad & |u| \leq 1 \text{ a.e. in } \Omega\,. && (29)
\end{aligned}$$

Given (23)-(24) we obtain $w - \fint_\Omega w = v$, i.e. v and w only differ by a constant. We can replace v by w in (25) and we hence obtain in particular a time discretization of (14), (15) using the complementary formulation (13). The Lagrange multiplier w coincides with the chemical potential, and the scaled Lagrange multiplier μ coincides with the subdifferential of $I_{[-1,1]}$. Since the equations (23) and (24) are not needed we omit them in the following.

In the following we consider the choice of $\psi_0(u) = \frac{1}{2}(1-u^2)$ and show that the system (25)-(29) has a solution. Defining the admissible set

$$\mathbf{U_{ad}} := \{u \in H^1(\Omega) \mid |u| \leq 1,\ \fint_\Omega u = m\}$$

(20) or respectively (21)-(22) can be reformulated as

$$\min_{u\in\mathbf{U_{ad}}} E(u) := \{\tfrac{\gamma\varepsilon}{2}\int_\Omega |\nabla u|^2 + \tfrac{1}{\varepsilon}\int_\Omega \psi_0(u) + \tfrac{1}{2\tau}\int_\Omega |\nabla(-\Delta)^{-1}(u-u^{n-1})|^2\}\,. \tag{30}$$

Since $\frac{1}{2}(1-u^2)$ is nonconvex the above minimization problem will in general omit more than one solution. But one can show that for small $\tau > 0$ the problem is uniquely solvable. This is the content of the following lemma. Similar restrictions on the time step in order to obtain uniqueness had to be imposed in a fully discrete situation in [3] and [8].

Lemma 2.1 *The minimization problem (30) has a solution. A unique solution exists if* $\tau \in (0, 4\gamma\varepsilon^3)$.

Proof: Since $|u| \leq 1$ we obtain that $\int\limits_\Omega \psi_0(u) = \int\limits_\Omega \frac{1}{2}(1-u^2)$ is non-negative and there exists a minimizing sequence $(u_k)_{k\in\mathbb{N}} \subset \mathbf{U_{ad}}$ for E, i.e.

$$E(u_k) \to \inf_{u\in\mathbf{U_{ad}}} E(u) > -\infty \quad \text{for} \quad k \to \infty\,.$$

Given that $(E(u_k))_{k\in\mathbb{N}}$ is uniformly bounded we can conclude that $\int\limits_\Omega |\nabla u_k|^2 dx$ is uniformly bounded. Due to $\int\limits_\Omega (u_k - m)dx = 0$ we can use Poincaré's inequality for functions with mean value zero, see e.g. [1], to obtain that $(u_k)_{k\in\mathbb{N}}$ is a bounded sequence in $H^1(\Omega)$. Using the fact that bounded sequences in $H^1(\Omega)$ have weakly converging subsequences and applying Rellichs theorem we obtain the existence of a subsequence such that

$$u_{k_j} \rightharpoonup u^* \text{ in } H^1(\Omega),\ u_{k_j} \to u^* \text{ in } L^2(\Omega) \text{ for } j \to \infty\,.$$

Since the terms $\int\limits_\Omega |\nabla u|^2 dx$ and $\int\limits_\Omega |\nabla(-\Delta)^{-1}u|^2 dx$ are convex, we obtain that they are weakly lower semi-continuous in $H^1(\Omega)$, see e.g. [19]. Since $\int\limits_\Omega \psi_0(u_{k_j})$ converges strongly we conclude that u^* is in fact a minimum of E in $\mathbf{U_{ad}}$.

The functional E is strictly convex on $\mathbf{U}$ if and only if $F(\eta) := E(\eta + u^{n-1})$ is strictly convex on $\mathbf{Y}$. Since F is the sum of terms which are constant or linear and of

$$\tfrac{\gamma\varepsilon}{2}\int\limits_\Omega |\nabla\eta|^2 - \tfrac{1}{2\varepsilon}\int\limits_\Omega \eta^2 + \tfrac{1}{2\tau}\int\limits_\Omega |\nabla(-\Delta)^{-1}\eta|^2 \tag{31}$$

we only need to show that (31) is strictly positive on $\mathbf{Y}\setminus\{0\}$. Using the definition of $(-\Delta)^{-1}$ and Young's inequality we obtain for all $\eta \in \mathbf{Y}$

$$\tfrac{1}{2\varepsilon}\int\limits_\Omega \eta^2 = \tfrac{1}{2\varepsilon}\int\limits_\Omega (\nabla(-\Delta)^{-1}\eta)\cdot\nabla\eta \leq \tfrac{\delta}{4\varepsilon}\int\limits_\Omega |\nabla(-\Delta)^{-1}\eta|^2 + \tfrac{1}{4\delta\varepsilon}\int\limits_\Omega |\nabla\eta|^2\,.$$

Choosing $\delta = \frac{2\varepsilon}{\tau}$ we obtain

$$\tfrac{\gamma\varepsilon}{2}\int\limits_\Omega |\nabla\eta|^2 - \tfrac{1}{2\varepsilon}\int\limits_\Omega \eta^2 + \tfrac{1}{2\tau}\int\limits_\Omega |\nabla(-\Delta)^{-1}\eta|^2 \geq \left(\tfrac{\gamma\varepsilon}{2} - \tfrac{\tau}{8\varepsilon^2}\right)\int\limits_\Omega |\nabla\eta|^2\,.$$

If $\tau < 4\gamma\varepsilon^3$ we obtain uniqueness from the strict convexity of E. □

Lemma 2.2 *A solution $u \in \mathbf{U_{ad}}$ of (30) solves the variational inequality*

$$\int\limits_\Omega \gamma\varepsilon\nabla u\cdot\nabla(\eta-u) - \tfrac{1}{\varepsilon}\int\limits_\Omega u(\eta-u) + \tfrac{1}{\tau}\int\limits_\Omega (-\Delta)^{-1}(u-u^{n-1})(\eta-u) \geq 0 \tag{32}$$

for all $\eta \in \mathbf{U_{ad}}$.

Proof: Computing the first variation of the first two terms in (30) in a direction $(\eta - u)$ is standard. In addition we have

$$\frac{d}{d\delta} \int\!\!\!\!\!\!-_{\Omega} |\nabla(-\Delta)^{-1}(u + \delta(\eta - u) - u^{n-1})|^2_{|\delta=0}$$
$$= \int\!\!\!\!\!\!-_{\Omega} \nabla(-\Delta)^{-1}(u - u^{n-1}) \cdot \nabla(-\Delta)^{-1}(\eta - u) = \int\!\!\!\!\!\!-_{\Omega} (-\Delta)^{-1}(u - u^{n-1})(\eta - u)\,.$$

Since the derivative of the functional in (30) has to be nonnegative in directions $\eta - u$ with $u \in \mathbf{U_{ad}}$ we obtain (32). □

Lemma 2.3 *Let $u \in \mathbf{U_{ad}}$ be a solution of the variational inequality (32). Then there exists a $\lambda \in \mathbb{R}$ such that for all $\eta \in H^1(\Omega)$ with $|\eta| \leq 1$ the inequality*

$$\begin{aligned} \int\!\!\!\!\!\!-_{\Omega} \gamma\varepsilon \nabla u \cdot \nabla(\eta - u) - \tfrac{1}{\varepsilon} \int\!\!\!\!\!\!-_{\Omega} u(\eta - u) \quad &+ \quad \tfrac{1}{\tau} \int\!\!\!\!\!\!-_{\Omega} (-\Delta)^{-1}(u - u^{n-1})(\eta - u) \\ &- \quad \lambda \int\!\!\!\!\!\!-_{\Omega} (\eta - u) \geq 0 \end{aligned} \tag{33}$$

holds.

Proof: We argue similar as in the proof of Proposition 3.3 in [7]. Let $f = \frac{2}{\varepsilon} u - \frac{1}{\tau}(-\Delta)^{-1}(u - u^{n-1})$. Since u and u^{n-1} are bounded by one in modulus we obtain from the theory of elliptic equations that f is bounded. We now define for each $\alpha \in \mathbb{R}$ a function $u_\alpha \in K := \{u \in H^1(\Omega) \mid |u| \leq 1\}$ such that for all $\eta \in K$

$$\int\!\!\!\!\!\!-_{\Omega} \gamma\varepsilon \nabla u_\lambda \cdot \nabla(\eta - u_\lambda) + \tfrac{1}{\varepsilon} \int\!\!\!\!\!\!-_{\Omega} u_\lambda(\eta - u_\lambda) \geq \int\!\!\!\!\!\!-_{\Omega} f(\eta - u_\lambda) + \alpha \int\!\!\!\!\!\!-_{\Omega} (\eta - u_\lambda)\,. \tag{34}$$

Using standard theory of variational inequalities we deduce that (34) has a unique solution, see e.g. [26]. We now introduce a function $M : \mathbb{R} \to \mathbb{R}$ by

$$M(\alpha) := \fint_{\Omega} u_\alpha\,.$$

For all $\eta \in K$ and all $\alpha \in \mathbb{R}$ we have the pointwise inequalities

$$(\tfrac{1}{\varepsilon} - f - \alpha)(\eta - 1) \geq (\tfrac{1}{\varepsilon} + \|f\|_\infty - \alpha)(\eta - 1)$$

$$\text{and} \quad \frac{1}{\varepsilon} - f - \alpha)(\eta + 1) \geq (-\tfrac{1}{\varepsilon} - \|f\|_\infty - \alpha)(\eta + 1)\,.$$

Hence $u \equiv 1$ is a solution of (34) if $\alpha \geq \frac{1}{\varepsilon} + \|f\|_\infty$ and $u \equiv -1$ is a solution of (34) if $\alpha \leq -(\frac{1}{\varepsilon} + \|f\|_\infty)$. We now obtain $M(\pm(\frac{1}{\varepsilon} + \|f\|_\infty)) = \pm 1$. As in the proof of Proposition 3.3 in [7] we obtain that M is monotone and continuous. Hence a $\overline{\lambda} \in \mathbb{R}$ exists such that $M(\overline{\lambda}) = m$. We now choose $\eta = u_{\overline{\lambda}}$ in (32) and $\eta = u$ in (34) with $\lambda = \overline{\lambda}$. Adding both resulting terms leads to

$$\int\!\!\!\!\!\!-_{\Omega} \gamma\varepsilon |\nabla(u - u_{\overline{\lambda}})|^2 + \tfrac{1}{\varepsilon} \int\!\!\!\!\!\!-_{\Omega} |u_{\overline{\lambda}} - u|^2 \leq 0\,,$$

where we use the fact that $\int_\Omega u = \int_\Omega u_{\overline{\lambda}}$. Hence $u = u_\lambda$. Using this result and the definition of f we conclude from (34) that u fulfills (33). □

Using regularity theory for obstacle problems we obtain similar as in the proof of Lemma 3.2 in [7]

$$u \in W^{2,p}_{loc}(\Omega) \text{ for all } p \in (1,\infty)\,, \quad u \in C^{1,\alpha}_{loc}(\Omega) \text{ for all } \alpha \in (0,1)\,.$$

Setting

$$\begin{aligned} v &= -(-\Delta)^{-1}\left(\frac{u-u^{n-1}}{\tau}\right),\ w = v+\lambda\,,\\ \mu_+ &= \varepsilon(\gamma\varepsilon\Delta u + \tfrac{1}{\varepsilon}u + w)^+\,,\\ \mu_- &= \varepsilon(\gamma\varepsilon\Delta u + \tfrac{1}{\varepsilon}u + w)^-\,,\\ \mu &= \mu_+ - \mu_- \end{aligned}$$

we obtain similar as for other optimization problems with bilateral constraints (see e.g. [34]) the following result.

Remark 2.1 *There exists a solution (u,v,w,μ) of the KKT system (23)-(29). In particular there is a Lagrange multiplier μ with $\mu \in L^2(\Omega)$. Replacing $\psi_0'(u)$ in (26) by $\psi_0'(u^{n-1})$ gives a semi-implicite time discretization, see e.g. [8]. Arguing similar as above a solution to the semi-discrete version exists which is in $H^2(\Omega)$. In this case the minimization problem related to (30) is always uniquely solvable, i.e. no restriction on the time step is necessary.*

3 Primal-dual active set approach

The goal of this section is to formulate a primal-dual active set method in order to solve for a time step $\tau > 0$ a spatially discretized version of

$$\tfrac{1}{\tau}(u-u^{n-1}) = \Delta w \text{ in } \Omega\,,\ \frac{\partial w}{\partial n} = 0 \text{ on } \partial\Omega \tag{35}$$

together with (26)-(29). We now introduce for a $\mathbf{c} > 0$ the active sets

$$A^+ = \left\{x \in \Omega \mid u(x) + \tfrac{\mu(x)}{\mathbf{c}} > 1\right\}, \qquad A^- = \left\{x \in \Omega \mid u(x) + \tfrac{\mu(x)}{\mathbf{c}} < -1\right\}$$

and the inactive set $I := \Omega\backslash(A^+ \cup A^-)$. The conditions (27)-(29) can be reformulated as

$$u(x) = \pm 1 \quad \text{if } x \in A^\pm\,, \qquad \mu(x) = 0 \qquad \text{if } x \in I\,. \tag{36}$$

Formally, this leads to the following primal-dual active set strategy employing the primal variable u and the dual variable μ.

Primal-Dual Active Set Algorithm (PDAS-I):

1. Set $k = 0$, initialize $A_0^{\pm}$ and define $I_0 = \Omega \setminus (A_0^+ \cup A_0^-)$.
2. Set $u_k = \pm 1$ on $A_k^{\pm}$ and $\mu_k = 0$ on I_k.
3. Solve the coupled system of PDE's (35), (26) to obtain u_k on I_k, μ_k on $A_k^+ \cup A_k^-$ and w_k on Ω.
4. Set $A_{k+1}^+ := \left\{ x \in \Omega \mid u_k(x) + \frac{\mu_k(x)}{\mathbf{c}} > 1 \right\}$,
   $A_{k+1}^- := \{ x \in \Omega \mid u_k(x) + \frac{\mu_k(x)}{\mathbf{c}} < -1 \}$ and $I_{k+1} = \Omega \setminus (A_{k+1}^+ \cup A_{k+1}^-)$.
5. If $A_{k+1}^{\pm} = A_k^{\pm}$ stop, otherwise set $k = k + 1$ and goto 2.

Another reformulation of (27)-(29) is given with the help of a semi-smooth equation as follows

$$H(u, \mu) := \mu - (\max(0, \mu + \mathbf{c}(u - 1)) + \min(0, \mu + \mathbf{c}(u + 1)) = 0 \,. \tag{37}$$

A semi-smooth Newton method applied in a formal way to (35), (26), (37) is equivalent to the above primal-dual active set method, see e.g. [23] for a different context. It is known that for obstacle problems the iterations in (PDAS-I) in general are not applicable in function space since the iterates μ_k are only measures and not L^2-functions, see [24]. The same is true for the non-standard obstacle problem (21), as Δu_k as obtained in the iterations of (PDAS-I) in general is only a measure. In the following section we introduce a finite element discretization of (25)-(29) and we show that for the discretized system local superlinear convergence holds.

4 Finite element discretization

We now introduce a finite element approximation for the Cahn-Hilliard variational inequality using continuous, piecewise affine linear finite elements for u and w. In the following we assume for simplicity that Ω is a polyhedral domain. Generalizations to curved domains are possible using boundary finite elements with curved faces. Let $\{\mathcal{T}_h\}_{h>0}$ be a triangulation of Ω into disjoint open simplices. Furthermore, we define $\mathcal{T}_h$ to have maximal element size $h := \max_{T \in \mathcal{T}_h} \{diam(T)\}$ and we set J_h to be the set of nodes of $\mathcal{T}_h$ and $p_j \in J_h$ to be the coordinates of these nodes. The finite element space of piecewise affine linear, continuous finite elements associated to $\mathcal{T}_h$ is now given as $S_h := \{\varphi \in C^0(\overline{\Omega}) \mid \varphi_{|T} \in P_1(T) \quad \forall\, T \in \mathcal{T}_h\} \subset H^1(\Omega)$ where we denote by $P_1(T)$ the set of all affine linear functions on T. To each $p_j \in J_h$ we associate the nodal basis function $\chi_j \in S_h$ with the property $\chi_j(p_i) = \delta_{ij}$. We replace the L^2-inner product $(.,.)_{L^2}$ at some places by a quadrature rule given by the lumped mass inner product $(\eta, \chi)_h = \int_\Omega I_h(\eta\chi)\,,$ where $I_h := C^0(\overline{\Omega}) \to S_h$ is the

standard interpolation operator at the nodes. In the following, we consider either an implicit or an explicit discretization of the term $\psi_0'(u)$, i.e. we choose $\psi_0'(u^*)$ where $* \in \{n-1, n\}$. Then, the spatial discretization of (35), (26)-(29) is given as:

For $n = 1, 2, 3, \ldots$ and given $u_h^0 \in S_h$ find iteratively $(u_h^n, w_h^n, \mu_h^n) \in S_h \times S_h \times S_h$ such that

$$\begin{aligned}
\tfrac{1}{\tau}(u_h^n - u_h^{n-1}, \chi)_h + (\nabla w_h^n, \nabla \chi) &= 0 \qquad \forall\ \chi \in S_h, \quad (38)\\
(w_h^n, \chi)_h - \gamma\varepsilon(\nabla u_h^n, \nabla \chi) - \tfrac{1}{\varepsilon}(\psi_0'(u_h^*), \chi)_h - \tfrac{1}{\varepsilon}(\mu_h^n, \chi)_h &= 0 \qquad \forall\ \chi \in S_h, \quad (39)\\
\mu_h^n = \mu_{h,+}^n - \mu_{h,-}^n\,, \quad \mu_{h,+}^n \geq 0\,, \quad \mu_{h,-}^n \geq 0\,, \quad |u_h^n| &\leq 1, \qquad (40)\\
\mu_{h,+}^n(p_j)(u_h^n(p_j) - 1) \;=\; \mu_{h,-}^n(p_j)(u_h^n(p_j) + 1) &= 0 \qquad \forall\ p_j \in J_h. \quad (41)
\end{aligned}$$

Notice that (41) does in general not imply (28) pointwise in all of Ω. Choosing $\chi \equiv 1$ in (38) provides the mass conservation $\fint\limits_\Omega u_h^n = \fint\limits_\Omega u_h^{n-1} = \fint\limits_\Omega u_h^0$.

The discretization of (27)-(29) can also be introduced as in Section 3 with the help of active nodes

$$\mathcal{A}_h^{n,+} = \left\{ p_j \in J_h \mid u_h^n(p_j) + \tfrac{\mu_h^n(p_j)}{\mathbf{c}} > 1 \right\},\ \mathcal{A}_h^{n,-} = \left\{ p_j \in J_h \mid u_h^n(p_j) + \tfrac{\mu_h^n(p_j)}{\mathbf{c}} < -1 \right\} \quad (42)$$

for any positive $\mathbf{c}$. Then we define the set of inactive nodes as $\mathcal{I}_h^n = J_h \backslash (\mathcal{A}_h^{n,+} \cup \mathcal{A}_h^{n,-})$ and require

$$u_h^n(p_j) = \pm 1 \quad \text{ if } p_j \in \mathcal{A}_h^{n,\pm}\,, \qquad \mu_h^n(p_j) = 0 \qquad \text{if } p_j \in \mathcal{I}_h^n. \quad (43)$$

As discussed in Sections 1 and 2 the equations (39), (42)-(43) can be rewritten as a variational inequality as follows. Introducing the space

$$K_h := \{\eta \in S_h \mid |\eta(x)| \leq 1 \quad \text{for all} \quad x \in \Omega\}\,.$$

we search $u_h^n \in K_h$ such that

$$(w_h^n, \xi - u_h^n)_h \geq \gamma\varepsilon(\nabla u_h^n, \nabla(\xi - u_h^n)) + \tfrac{1}{\varepsilon}(\psi_0'(u_h^{n-1}), \xi - u_h^n)_h \qquad \forall\ \xi \in K_h\,, \quad (44)$$

In order to compute (u_h^n, w_h^n, μ_h^n) we now choose a discretized version of the primal-dual active set method (PDAS-I), where we iteratively update active sets $\mathcal{A}_{h,k}^{n,\pm}$ for $k = 0, 1, 2, \ldots$. We drop for convenience sometimes the indices n, h. The following discrete version of the primal-dual active set strategy is obtained using that $\mu_h^n(p_j) = 0$ on $\mathcal{I}_{h,k}^n$ in (39). Then (39) reduces roughly spoken to a discretized PDE for u_h^n only on an interface determined by $\mathcal{I}_{h,k}^n$. For determined u_h^n, w_h^n (39) determines μ_h^n on the active set. Here one has to use that $(\cdot,\cdot)_h$ is a mass lumped L^2-inner product to uncouple (39) in active and inactive. For the precise formulation we introduce the notation

$$\tilde{S}_{h,k} := \{\tilde{\chi} \in S_h \,|\, \tilde{\chi}(p_j) = 0 \text{ if } p_j \in \mathcal{A}_{h,k}^{n,+} \cup \mathcal{A}_{h,k}^{n,-}\} = span\{\chi_i \mid p_i \in \mathcal{I}_{h,k}^n\}.$$

Primal-Dual Active Set Algorithm (PDAS-II):

1. Set $k=0$, initialize $\mathcal{A}_0^{\pm}$ and define $\mathcal{I}_0 = J_h \setminus (\mathcal{A}_0^+ \cup \mathcal{A}_0^-)$.

2. Solve for $(u_k, w_k) \in S_h \times S_h$ the system

$$\begin{aligned} \tfrac{1}{\tau}(u_k - u_h^{n-1}, \chi)_h + (\nabla w_k, \nabla \chi) &= 0 \qquad \forall\ \chi \in S_h\,, && (45)\\ (w_k, \tilde{\chi})_h - \gamma\varepsilon(\nabla u_k, \nabla \tilde{\chi}) - \tfrac{1}{\varepsilon}(\psi_0'(u_h^*), \tilde{\chi})_h &= 0 \qquad \forall\ \tilde{\chi} \in \tilde{S}_{h,k}\,, && (46)\\ u_k(p_j) &= \pm 1 \quad \text{if } p_j \in \mathcal{A}_k^{\pm}\,. && (47) \end{aligned}$$

3. Define $\mu_k \in S_h$ via

$$\begin{aligned} \mu_k(p_j)\,(1, \chi_j)_h &= \varepsilon(w_k, \chi_j)_h - \gamma\varepsilon^2(\nabla u_k, \nabla \chi_j) - (\psi_0'(u_h^*), \chi_j)_h \quad \forall\ p_j \notin \mathcal{I}_k, && (48)\\ \mu_k(p_j) &= 0 \qquad \forall\ p_j \in \mathcal{I}_k. && (49) \end{aligned}$$

4. Set $\mathcal{A}_{k+1}^+ := \{p_j \in J_h \mid u_k(p_j) + \frac{\mu_k(p_j)}{\mathbf{c}} > 1\}$, (50)
$\mathcal{A}_{k+1}^- := \{p_j \in J_h \mid u_k(p_j) + \frac{\mu_k(p_j)}{\mathbf{c}} < -1\}$ and $\mathcal{I}_{k+1} = J_h \setminus (\mathcal{A}_{k+1}^+ \cup \mathcal{A}_{k+1}^-)$. (51)

5. If $\mathcal{A}_{k+1}^{\pm} = \mathcal{A}_k^{\pm}$ stop, otherwise set $k = k+1$ and goto 2.

Lemma 4.1 *For all $u_h^{n-1} \in S_h$ and $\mathcal{A}_k^{\pm}$ there exists a unique solution $(u_k, w_k) \in S_h \times S_h$ of (45)-(47) with $* = (n-1)$, i.e. the semi-implicit case, provided that $\mathcal{I}_k = J_h \setminus (\mathcal{A}_k^+ \cup \mathcal{A}_k^+) \neq \emptyset$.*

Proof: The idea of this proof is to consider the discretized version of (21) and (22) under the constraint $u = \pm 1$ on $\mathcal{A}_k$ and follow the existence proof as in Section 3. Hence, we define $S_{h,m} := \{\chi \in S_h \mid \fint_\Omega \chi = m\}$, where $m := \fint_\Omega u_h^{n-1}$,

$$S_h^I := \{u \in S_h \mid u(p_j) = 1 \text{ if } j \in \mathcal{A}_k^+, u(p_j) = -1 \text{ if } j \in \mathcal{A}_k^-\}\,,$$

and $S_{h,m}^I := S_h^I \cap S_{h,m}$. Since $\mathcal{I}_k \neq \emptyset$ we conclude $S_{h,m}^I \neq \emptyset$. The discrete inverse Laplacian $(-\Delta_h)^{-1} : S_{h,0} \to S_{h,0}$, $\eta^h \mapsto (-\Delta_h)^{-1}\eta^h$ is defined via

$$(\nabla((-\Delta_h)^{-1}\eta^h), \nabla\chi) = (\eta^h, \chi)_h \quad \text{for all} \quad \chi \in S_{h,0}\,. \tag{52}$$

Since the homogeneous problem only has the trivial solution and $S_{h,0}$ is finite dimensional, the linear equation (52) has a unique solution. We define $u_k \in S_{h,m}^I$ as the solution of the minimization problem

$$\min_{\eta \in S_{h,m}^I} \{\tfrac{1}{2\tau}(\nabla(-\Delta_h)^{-1}(\eta - u_h^{n-1}), \nabla(-\Delta_h)^{-1}(\eta - u_h^{n-1})) + \tfrac{\gamma\varepsilon}{2}(\nabla\eta, \nabla\eta) + \tfrac{1}{\varepsilon}(\psi_0'(u_h^{n-1}), \eta)_h\} \tag{53}$$

which exists uniquely since the Poincaré inequality similar as in the proof of Lemma 2.1 implies coerciveness. Computing the first variation of the minimisation problem

(53) gives for $u_k \in S^I_{h,m}$

$$0 = \tfrac{1}{\tau}(\nabla(-\Delta_h)^{-1}(u_k - u_h^{n-1}), \nabla(-\Delta_h)^{-1}\tilde{\chi}) + \gamma\varepsilon(\nabla u_k, \nabla\tilde{\chi}) + \tfrac{1}{\varepsilon}(\psi_0'(u_h^{n-1}), \tilde{\chi})_h \quad (54)$$

for all $\tilde{\chi} \in \tilde{S}_{h,k}$ with $\fint\limits_\Omega \tilde{\chi} = 0$. Now we define $w_k \in S_h$ as

$$w_k = -(-\Delta_h)^{-1}\left(\frac{u_k - u_h^{n-1}}{\tau}\right) + \lambda_k \quad (55)$$

where $\lambda_k \in \mathbb{R}$ is uniquely given by any nodal basis function $\chi_j \in S_h$ with $p_j \in \mathcal{I}_k$ by

$$\lambda_k = \{\tfrac{1}{\tau}((-\Delta_h)^{-1}(u_k - u_h^{n-1}), \chi_j)_h + \gamma\varepsilon(\nabla u_k, \nabla\chi_j) + \tfrac{1}{\varepsilon}(\psi_0'(u_h^{n-1}), \chi_j)\}/(1, \chi_j). \quad (56)$$

Using the definition of the discrete inverse Laplacian, see (52) and the fact that $\fint\limits_\Omega u_k = \fint\limits_\Omega u^{n-1}$ now gives that (45) holds. Furthermore (54), (52) and (55) imply that (46) holds for all $\tilde{\chi} \in \tilde{S}_{h,k}$ with $\fint\limits_\Omega \tilde{\chi} = 0$. For $\tilde{\chi} \in \tilde{S}_{h,k}$ which do not satisfy the integral constraint $\fint\limits_\Omega \tilde{\chi} = 0$ we set $\hat{\chi} := \tilde{\chi} - \alpha\chi_j$ with $p_j \in I_k$ and $\alpha \in \mathbb{R}$ such that $\int\limits_\Omega \hat{\chi} = 0$. With this choice of $\hat{\chi}$ as a test function in (54) we can conclude with the help of (52), (55) and (56) that (46) holds for all $\tilde{\chi} \in \tilde{S}_{h,k}$. Hence (45)-(47) has a solution.

It remains to prove uniqueness. Let us assume that (45)-(47) has two solutions $(u_{k,1}, w_{k,1}), (u_{k,2}, w_{k,2}) \in S_h \times S_h$. Then we obtain for the differences $v = u_{k,1} - u_{k,2}$, $z = w_{k,1} - w_{k,2}$ by testing (45), (46) for $(u_{k,1}, w_{k,2})$ and $(u_{k,2}, w_{k,2})$ with v and z respectively, after taking differences:

$$(v, z)_h + \tau\|\nabla z\|^2_{L^2} - (z, v)_h + \gamma\varepsilon\|\nabla v\|^2_{L^2} = 0\,.$$

Since $\fint\limits_\Omega u_{k,1} = \fint\limits_\Omega u_{k,2} = \fint\limits_\Omega u^{n-1}$ we obtain $v \equiv 0$ in Ω and hence $u_{k,1} = u_{k,2}$. The identities (45), (46) imply that necessarily the identities (55) and (56) have to hold. This implies that also w_k is unique. □

Now μ_k is uniquely defined by (48), (49) and hence taking Lemma 4.1 into account we obtain that a unique solution of (45)-(49) exists.

In the following we require the condition $\mathcal{I}_k = J_h \setminus (\mathcal{A}_k^+ \cup \mathcal{A}_k^-) \neq \emptyset$, which guarantees that there is a $u \in S_h$ which can fulfill $\fint\limits_\Omega u = m$. Otherwise (45) is not solvable.

Remark 4.1 *In order to solve* (45)-(49) *the main computational effort is to solve the system* (45), (46) *which has a specific structure. The discretized elliptic equation* (45) *for* w *is defined on the whole of* Ω *whereas the elliptic equation* (46) *is defined only on the inactive set, see Figure* 1. *The two equations are coupled in a way*

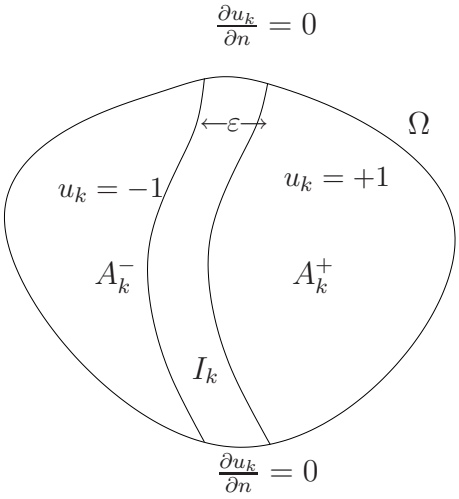

Figure 1: The system (45)-(46) leads to an equation for u_k on the inactive set $\mathcal{I}_k$ and for w_k on the whole of Ω.

which leads to an overall symmetric system which will be used later when we propose numerical algorithms.

The discretization of (27)-(29) can also be formulated with the help of the semi-smooth function H, see (37), as a nonlinear equation

$$H(u_h^n(p_j), \mu_h^n(p_j)) = 0 \qquad \forall\ p_j \in J_h\,. \tag{57}$$

Using the approach of [23] we can interpret (PDAS-II) as a semi-smooth Newton method for the system (38), (39), (57) and the following local convergence result for the semi-implicit discretization.

Theorem 4.1 *Let $(u, w, \mu) \in S_h \times S_h \times S_h$ be a solution of (38), (39), (57) with $* = (n-1)$ such that $\{p_j \in J_h \mid |u(p_j)| < 1\} \neq \emptyset$. Then the semi-smooth Newton method for (38), (39), (57) and hence (PDAS-II) converges superlinearly in a neighborhood of (u, w, μ).*

Proof: Showing the existence of a solution to (38), (39), (57) is equivalent to the problem of finding a zero of the mapping

$$G : S_h \times S_h \times S_h \to S_h \times S_h \times S_h$$

where for $(u, w, \mu) \in S_h \times S_h \times S_h$ we define $G = (G_1, G_2, G_3)$ via

$$\begin{aligned}
(G_1(u, w, \mu), \chi)_h &:= (u - u_h^{n-1}, \chi)_h + \tau(\nabla w, \nabla \chi)\,, \\
(G_2(u, w, \mu), \chi)_h &:= (w, \chi)_h - \gamma\varepsilon(\nabla u, \nabla \chi) - \tfrac{1}{\varepsilon}(\psi_0'(u_h^{n-1}), \chi)_h - \tfrac{1}{\varepsilon}(\mu, \chi)_h\,, \\
(G_3(u, w, \mu), \chi)_h &:= (H(u, \mu), \chi)_h\,.
\end{aligned}$$

The min-max-function $H(u, \mu)$ is slantly differentiable and a slanting function is given by $DH(u, \mu) = (0, 1)$ if $|u + \frac{\mu}{c}| \leq 1$ and $DH(u, \mu) = (-c, 0)$ otherwise,

(see [22]). As a consequence G is slantly differentiable. Moreover similar as in [22] we can derive that the primal-dual active set method (PDAS-II) is equivalent to a semi-smooth Newton method for G. We now get local superlinear convergence of (PDAS-II) if we can show that the slanting function of G is invertible in a suitable neighbourhood of (u, w, μ) and the inverses are uniformly bounded ([11, 23]).

The semi-smooth derivative (slanting function) of G is invertible at $(\hat{u}, \hat{w}, \hat{\mu}) \in S_h \times S_h \times S_h$ if and only if we can show injectivity, i.e. that a unique solution $(\overline{u}, \overline{w}, \overline{\mu}) \in S_h \times S_h \times S_h$ of the following linear system exists

$$(\overline{u}, \chi)_h + \tau(\nabla \overline{w}, \nabla \chi) = 0, \ \forall \chi \in S_h \,, \tag{58}$$

$$(\overline{w}, \chi)_h - \gamma\varepsilon(\nabla \overline{u}, \nabla \chi) - \tfrac{1}{\varepsilon}(\overline{\mu}, \chi)_h = 0, \ \forall \chi \in S_h \,. \tag{59}$$

$$\overline{u}(p_j) = 0 \quad \text{if} \quad p_j \in \hat{\mathcal{A}} := \left\{ p_j \in J_h \mid \left| \hat{u}(p_j) + \frac{\hat{\mu}(p_j)}{c} \right| > 1 \right\} , \tag{60}$$

$$\overline{\mu}(p_j) = 0 \quad \text{if} \quad p_j \in \hat{\mathcal{I}} := J \setminus \hat{\mathcal{A}} \,, \tag{61}$$

Testing (58) with $\overline{w}$, (59) with $\overline{u}$ and using $(\overline{\mu}, \overline{u})_h = 0$ we obtain

$$\tau(\nabla \overline{w}, \nabla \overline{w}) + \gamma\varepsilon(\nabla \overline{u}, \nabla \overline{u}) = 0 \,. \tag{62}$$

This implies that $\overline{u}$ and $\overline{w}$ are constant. Then (58) gives $\overline{u} \equiv 0$. Using the fact that there exists a $p_j \in J_h$ with $|u(p_j)| < 1$ and $\mu(p_j) = 0$ we can guarantee that $\hat{\mathcal{I}} \neq \emptyset$ for $(\hat{u}, \hat{w}, \hat{\mu})$ out of a suitable neighborhood of (u, w, μ). Hence testing in (59) with χ_j where $p_j \in J_h$ implies $\overline{w} \equiv 0$ and finally (61) and (59) yield $\overline{\mu} \equiv 0$.

The semi-smooth derivatives only differ if the active and inactive sets change. Since only a finite number of different choices of these sets are possible we obtain that the inverses are uniformly bounded for all $(\hat{u}, \hat{w}, \hat{\mu})$ with a non-vanishing inactive set $\hat{\mathcal{I}}$. Since we can find an open neighborhood of (u, w, μ), where the condition $\hat{\mathcal{I}} \neq \emptyset$, we proved the theorem. □

Remark 4.2 *Let (u, w, μ) be a solution to (38), (39), (57). The proof of Theorem 4.1 requires a neighborhood of (u, w, μ), where the active sets do not vanish. This can limit the size of the neighborhood in which local superlinear convergence can be guaranteed. However in numerical simulations the mesh size always has to be chosen such that at least eight points lie across the interface. Hence the above mentioned condition never led to any problems in practice.*

Remark 4.3 *Theorem 4.1 holds also for the implicit discretization if $\tau \leq 4\gamma\varepsilon^3$.*

Proof: The proof follows align with 4.1 if one can show injectivity. Equation (59) changes to

$$(\overline{w}, \chi)_h - \gamma\varepsilon(\nabla \overline{u}, \nabla \chi) - \tfrac{1}{\varepsilon}(\overline{\mu}, \chi)_h + \tfrac{1}{3}(\overline{u}, \chi)_h = 0$$

The same testing as above leads to $\tau(\nabla \overline{w}, \nabla \overline{w}) + \gamma\varepsilon(\nabla \overline{u}, \nabla \overline{u}) - \frac{1}{\varepsilon}(\overline{u}, \overline{u})_h = 0$ and testing (58) with $\overline{u}$ yields $(\overline{u}, \overline{u})_h = \tau(\nabla \overline{w}, \nabla \overline{u})$. Then, if $\tau \leq 4\gamma\varepsilon^3$ we obtain with Young's inequality injectivity. □

5 Numerical results

In this section we discuss four test examples and numerically analyse the behaviour of the PDAS-algorithm. In the first test example we consider two concentric circles, where the exact sharp interface solution is known, and compare semi-implicit and implicit discretization.

The second example is a four-circle problem where concave as well as convex sections appear in the interface. Time evolution is given not only for u but also for w and the Lagrange multiplier μ. With this example we compare the PDAS-method with a standard solver for the Cahn-Hilliard inequality, namely with a projected block Gauss-Seidel method [4]. It turns out that the PDAS-method is more efficient and reliable. In particular, the speed up is gained by a linear algebra solver which is not based on a Gauss–Seidel method. Moreover, we have not seen a difference in CPU-time between the semi-implicit and implicit discretization, and in the latter case have not faced such a severe restriction on the time step τ as indicated by the analysis. The number of PDAS-iterations for each time step were rather depending on τ than on the mesh size h, never exceeded 11 and after the interface settles $2-4$ iterations were sufficient. For the number of iterations there was nearly no difference between an adaptive and a uniform grid. But of course in CPU-time adaptivity was much more efficient. In the third test example we considered random initial data, i.e. a starting situation without pure phases. Here and in our last example, a 3D simulation, we observed that even with large topological changes the maximum number of PDAS-iterations stayed always below 10.

Before we present the examples we discuss some numerical issues as there are mesh generation, adaptivity in order to resolve the interface, choice of the parameter c, initialization of the active sets and the linear algebra solver. Also we describe shortly the mentioned projected Gauss–Seidel type algorithm.

1. Mesh generation and adaptivity

For all the simulations presented in this paper the finite element toolbox ALBERTA [35] was used for mesh generation, the assembly of the matrices and administration. To generate the adaptive meshes we used the mesh adaption strategy of Barrett, Nürnberg, Styles [4]. Experiments showed that it is essential to ensure that at least eight vertices are present on the interfaces to avoid mesh effects, see also [9]. We hence refine on the interface down to a level where eight vertices are present and coarse in the areas where the concentration $\mathbf{u}$ is constant. For given parameters ε and γ this results in an upper bound $h_{fine} \leq \varepsilon\sqrt{\gamma}\frac{\pi}{9}$, where h_{fine} is the refinement level on the interface. Since we want to avoid too coarse meshes we additionally define $h_{coarse} := 10 \cdot h_{fine}$ and choose a tolerance tol. Afterwards the mesh adaption is done the following way: For each element $T \in \mathcal{T}^h$ calculate the indicator $\eta_T := |\min_{x\in T} |\mathbf{u}(x)| - 1|$. Then, a triangle is marked for refinement if it, or one of its neighboring elements, satisfies $\eta_T > tol \cdot 10^{-1}$ and if $h_T > h_{fine}$. A triangle is

marked for coarsening if it satisfies $\eta_T < tol \cdot 10^{-3}$ and $h_T < h_{coarse}$.

2. Choice of the parameter $\mathbf{c}$

To determine the active sets we have to choose the parameter $\mathbf{c} > 0$. In the unilateral case the selection of $\mathbf{c} > 0$ has no influence on the iterates after the first iteration and can be chosen arbitrary, see [23]. However this is no longer true in the case of bilateral bounds. This is discussed for obstacle problems in [6]. If $\mathbf{c}$ is chosen too small we observe cases in which the iterates oscillated and the algorithm did not converge. Figure 2 shows the values of u at various PDAS iterations in one time step of a simulation in one space dimension with $h = \frac{1}{512}$, $\tau = 10^{-5}$, $\pi\varepsilon = 0.2$ and $\mathbf{c} = 0.01$. In the 8th iteration the algorithm breaks down because all vertices are in

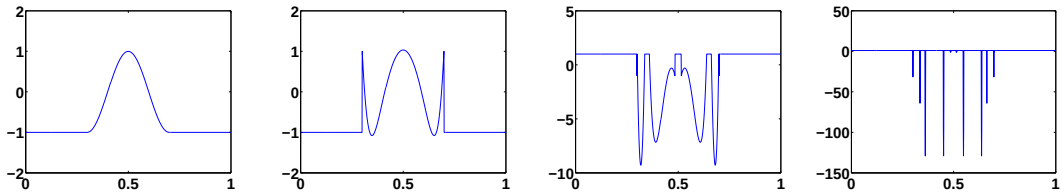

Figure 2: Oszillations in 1D if $\mathbf{c}$ is too small.

the active set and the system no longer exhibits a valid solution, compare Remark 4.1. Redoing the simulation with $\mathbf{c} = 0.2$ fixed the problem and after two iterations the time step was completed with only marginal changes to u since the initial data was close to a stationary solution. The same phenomenon was observed in higher space dimensions.

A heuristic approach showed that it is sufficient to ensure that no vertex can change from the positive active set $\mathcal{A}^+$ to the negative inactive set $\mathcal{A}^-$ and vice versa in one iteration. This can be achieved by selecting a PDAS parameter $\mathbf{c}$ large enough, depending on the magnitude of the Lagrange multiplier μ.

In all the simulations a value of $\mathbf{c} = 10$ was sufficient when the interfaces were already well developed and adequate initial guesses for the active sets were known. Therefore, if not mentioned otherwise $\mathbf{c} = 10$ is chosen in the calculation. In simulations with distortions or jumps in the concentration u larger values depending on the mesh size were necessary. Choosing the parameter $\mathbf{c}$ larger had no discernible influence on the simulation.

When using adaptive meshes for the PDAS algorithm a choice has to be made for every newly created vertex if it should belong to the active or inactive set. For now we restrict ourselves to the following: If all neighboring vertices are active then this vertex should be active too. In every other case we set the new vertex to inactive.

3. Initialization of active sets

As mentioned previously the application of a PDAS-method to the interface evolution has the advantage that the good initialization due to the information of the

previous time step leads to a large speedup. At the first time step $n = 1$ the active set $\mathcal{A}_0^{n,\pm}$ is initialized using the given initial data u_h^0. Since in the limit the active sets describe the sets where u is strictly active a good approximation of $\mathcal{A}_0^{1,\pm}$ is given by the active set of u_h^0. Hence we choose $\mathcal{A}_0^{1,\pm} = \{p_j \in S^h \mid |u_h^0(p_j) \mp 1| \leq 10^{-8}\}$.

For time steps $n \geq 2$ we can exploit in addition $\mu_{h_{n-1}}^{n-1}$. Due to possible grid changes from time step $n-1$ to time step n one may have to apply additionally the standard interpolation I_{h_n} to the new grid S_{h_n}, i.e. with $u_{-1} := I_{h_n} u_{h_{n-1}}^{n-1}$ and $\mu_{-1} := I_{h_n} \mu_{h_{n-1}}^{n-1}$ initialize the active set $\mathcal{A}_0^{n,\pm}$ as in (50) and (51). However less time consuming to initialize the active set is the following way, which is applied in this paper: if an edge between two positive or two negative active vertices is bisected, choose the new vertex is set respectively active and otherwise set the new vertex as inactive.

4. Solver for the equation system (45)-(46)

For moderate mesh sizes direct solvers for sparse equation systems perform quite well. We use a Cholesky decomposition of the system by means of the multifrontal method by Duff and Reid [17] which is realized in the software package the UMFpack [13], [14]. This method is a generalization to the frontal method of Irons [25]. One crucial point of this method is that the decomposition steps of the matrix are computed but not directly applied to the system matrix. Furthermore an elimination tree and pivoting strategy are used which make use of the sparsity of the system. For further discussion of the method refer to [28], [15]. We solved the whole reduced symmetric sparse system (45)-(46) with (47) by UMFpack all at once.

Up to now in our numerical experiments this direct solver performed better than e.g. a block SOR method. The application of other methods like, for example a cg-method for a preconditioned Schur-Complement or block multigrid method, are currently under investigation. In the first tests, which were of moderate size, UMFpack was still faster. The limit of the UMFpack up to now was the available memory. However large 3D problems have not been investigated yet thoroughly.

5. Gauss–Seidel type algorithm for the variational inequality (pSOR)

The following Gauss–Seidel type algorithm is often used for solving the Cahn-Hilliard variational inequality, see [31], and is implemented in the same hardware and software environment as our method. Hence to obtain a comparison within the same setting we use this method as a reference method. This method is based upon the discretization of the variational inequality (16)-(17) by a semi-implicit backwards Euler method in time and by using continuous piecewise linear elements in space, compare [8]. This results in the same discretization as we introduced in this paper, namely (38) and (44):

For $n = 1, 2, 3, ...$ and given $u_h^0 \in K_h$ find $(u_h^n, w_h^n) \in K_h \times S_h$ such that

$$\begin{aligned} \tfrac{1}{\tau}(u_h^n - u_h^{n-1}, \chi)_h + (\nabla w_h^n, \nabla \chi) = &\quad 0 \quad \forall\, \chi \in S_h, \\ \gamma\varepsilon(\nabla u_h^n, \nabla(\xi - u_h^n)) - (w_h^n, \xi - u_h^n)_h + \tfrac{1}{\varepsilon}(\psi_0'(u_h^{n-1}), \xi - u_h^n)_h \geq &\quad 0 \quad \forall\, \xi \in K_h\,. \end{aligned}$$

As is known for obstacle problems (see e.g. [31]) one can apply for this nonstandard variational inequality a projected block-Gauss-Seidel or a projected block-SOR method (pSOR). This has been studied in [4], where also convergence has been shown. The blocks are determined by the 2×2 blocks corresponding to the values $(u_h^n(p_j), w_h^n(p_j))$, which are merged for each vertex. In our numerical experiments we use the pSOR-method with overrelaxation using $\omega = 1.3$ for comparison with the PDAS-method. As stopping criteria $\|u_k - u_{k-1}\|_2 \leq 10^{-7}$ and a maximum of 50000 iterations is used.

5.1 Test cases

Example 1: Two concentric circles

The distinction we made in Section 4 between the explicit and implicit discretization of the free energy term leads to differences in the evolution process. We use a radial symmetric situation where the exact sharp interface solution is known to compare these two schemes. The initial data are such that the interface is described by two concentric circles with radii $0 < r_1(0) = 0.05 < r_2(0) = 0.15 < 1$. They both will shrink over time -the smaller faster than the larger circle- until the smaller one vanishes. Then the solution remains stable due to mass conservation.

In the limit $\varepsilon \to 0$ the Cahn–Hilliard model describes the evolution of the sharp interface Mullins–Sekerka model, see [9], [32]. The radial symmetric sharp interface solution is discussed in [36], [12]. In above situation the exact sharp interface solution can be calculated as solution of an ODE

$$r_1' = -\frac{1}{r_1}\frac{\sigma}{r_1 r_2}\frac{r_1 + r_2}{ln(r_1) - ln(r_2)}, \quad r_2' = -\frac{1}{r_2}\frac{\sigma}{r_1 r_2}\frac{r_1 + r_2}{ln(r_1) - ln(r_2)}$$

where $\sigma = \frac{\pi}{8}$. For the comparison between the semi-implicit and implicit discretization we used an equidistant mesh. In Figure 3 we plotted the sum of both radii for fixed $\varepsilon = 0.0039$ and varying time step width τ . In the implicit case we can choose even larger τ and already gain a good approximation of the evolution unlike for the semi-implicit case where a smaller time step width is necessary to achieve the desired result. This has been also observed when considering the convergence with respect to ε to the sharp interface with a fixed time step. The time step can be chosen larger in the implicit case.

Example 2: 4-circles problem

In this example we realize a concave as well as a convex section of the interface, which is a situation of large interest. The initial data on $\Omega = (0, 1)^2$ consist of four circular interfaces of width $\varepsilon\pi$. The centres and radii are chosen in such a way that three of circles intersect and one is detached. The values ± 1 are connected by a sine profile which is given as the lowest order term in an asymptotic expansion of the Cahn-Hilliard variational inequality, see e.g. [9]. In Figure 4 we show the inital data

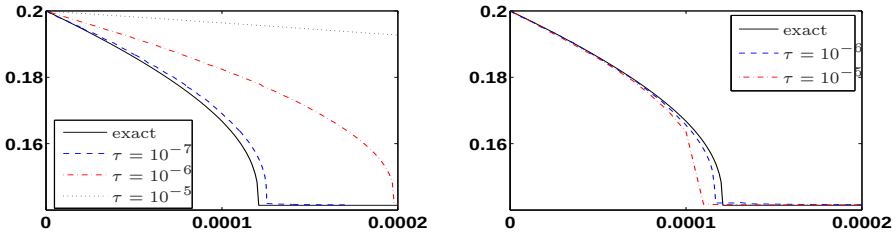

Semi-implicit Implicit

Figure 3: $(r_1 + r_2)(t)$ for different τ with $\varepsilon = 0.0039$.

for two different interface width. The initial active sets show a value of 0 on each inactive vertex and a positive resp. negative value on each active vertex. We set

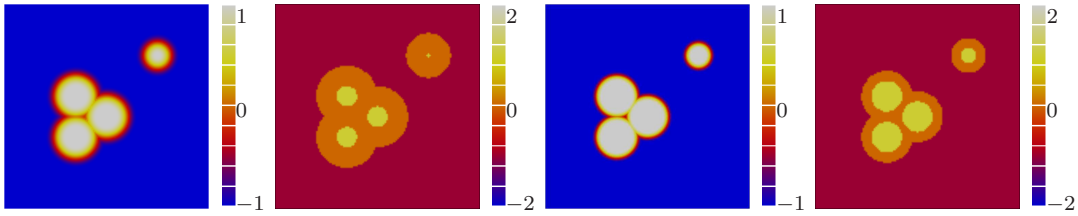

u_h^0 $\mathcal{A}_h^{0,\pm}, \mathcal{I}_h^0$ u_h^0 $\mathcal{A}_h^{0,\pm}, \mathcal{I}_h^0$

Figure 4: Initial data for $\pi\varepsilon = 0.1$ (left) and $\pi\varepsilon = 0.05$ (right).

$T_{end} = 0.02$ for all the following simulations. In Figure 5 and Figure 6 the evolution of u, w and μ in time is plotted. Here we used a semi-implicit discretization with an adaptive mesh with $h_{fine} = 0.01$ for $\pi\varepsilon = 0.1$ and $h_{fine} = 0.005$ for $\pi\varepsilon = 0.05$ respectively, the time step $\tau = 10^{-5}$. Simulations with equidistant mesh give the same results. The columns from left to right show the values of u, w, μ and the mesh after 5, 50, 100, 110 and 200 time steps.

Table 1 shows that for a small number of vertices the pSOR algorithm is still fast but with an increasing number of vertices its performance quickly deteriorates. Using the corresponding block SOR-method in combination with the PDAS-method, the resulting solver is even a bit slower for large time steps. The direct solver on the other hand lowers the runtime extremly. Moreover we see that there is nearly no difference in CPU-time between semi-implicit and implicit discretization. The severe restriction on the time step for the implicit case as stated in Lemma 2.1 has not been observed. Only for $\pi\varepsilon = 0.05$ the choice $\tau = 10^{-4}$ failed even for very large parameter $\mathbf{c} = 10^{10}$.

When we compare the runtimes used on the fixed mesh with 16641 vertices we notice that the simulations with $\pi\varepsilon = 0.2$ used up almost double the time of the one with $\pi\varepsilon = 0.1$. The reason lies in the size of the inactive set, which is roughly spoken the interface with width $\pi\varepsilon$. Hence for $\pi\varepsilon = 0.2$ the system (45)-(46) which has to be solved is of larger dimension.

In addition in Table 1 the total, the averaged and the maximal number of PDAS-iterations are listed for the semi-implicit discretization. The numbers for the implicit

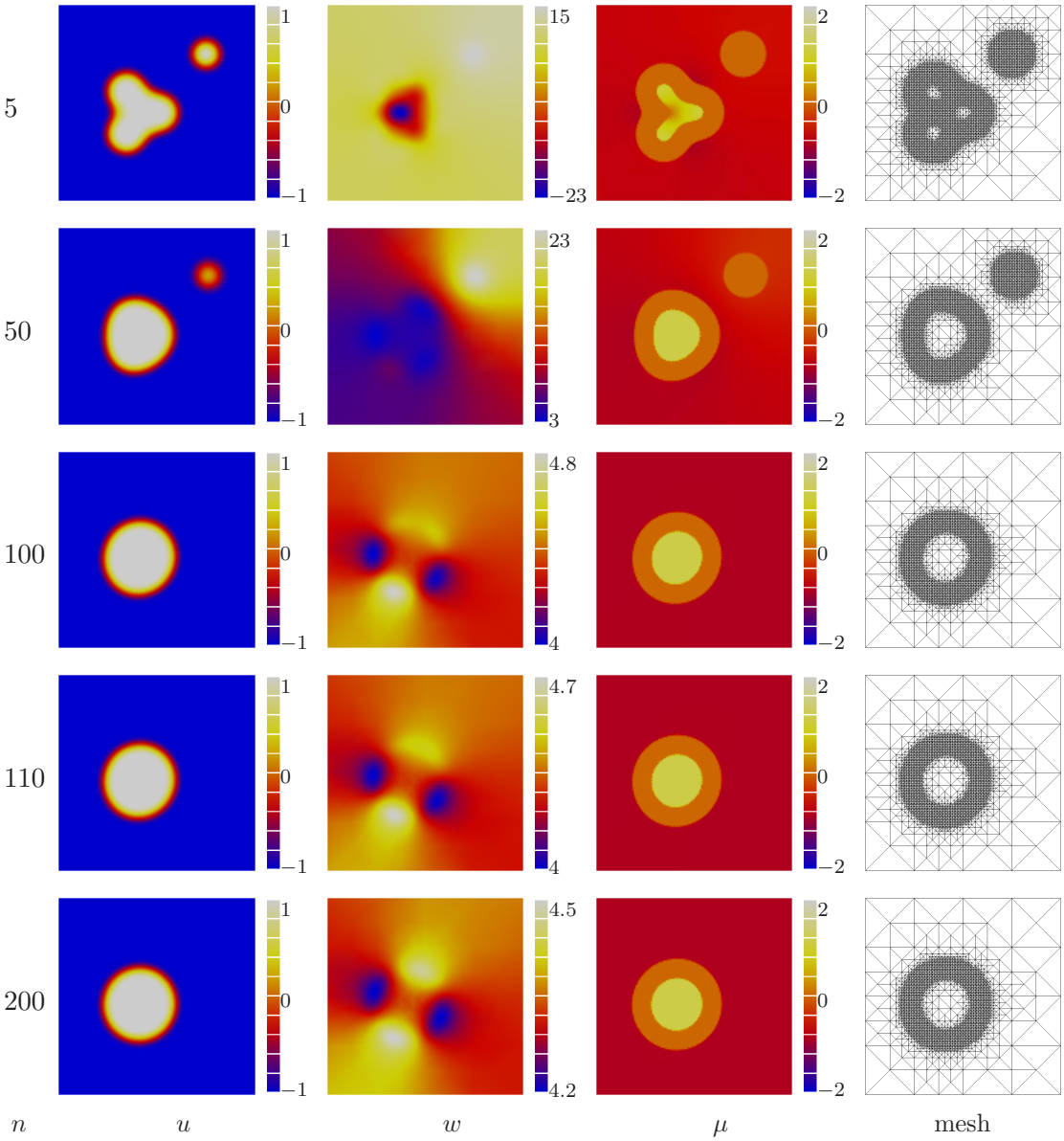

Figure 5: Time evolution of Example 2 with $\pi\varepsilon = 0.1$.

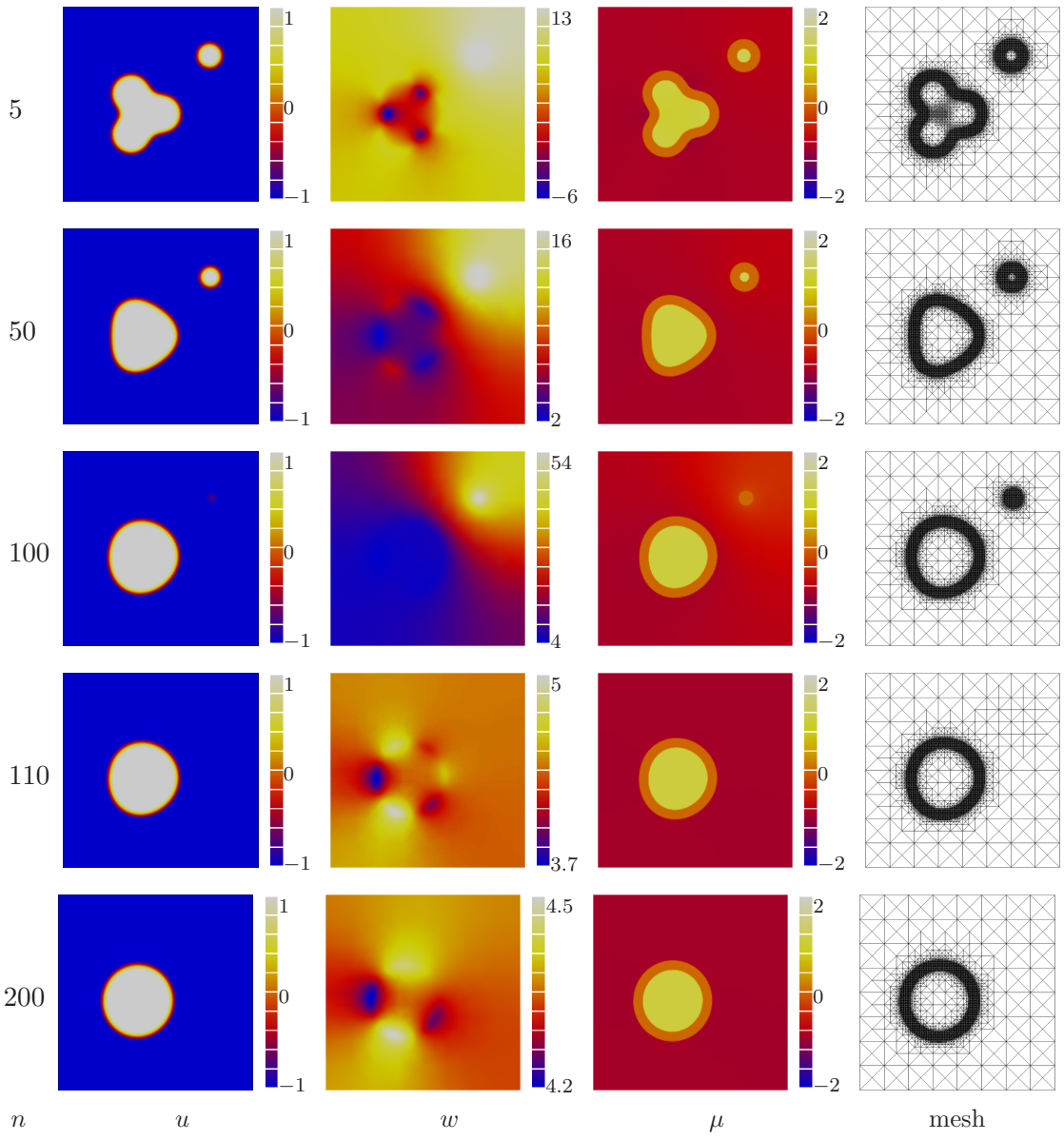

Figure 6: Time evolution of Example 2 with $\pi\varepsilon = 0.05$.

$\pi\varepsilon$	h	τ	CPU–Time in seconds			PDAS-iterations		
				semi-impl.	impl.			
	($\mathcal{J}$)		pSOR	PDAS	PDAS	total	average	max
0.2	0.02210	10^{-4}	57.1	10.7	11.2	74	3.5	5
	(4225)	10^{-5}	270.9	29.7	63.6	450	2.2	4
		10^{-6}	703.3	195.0	202.6	2958	1.5	3
	0.01105	10^{-4}	1071.6	69.4	39.5	100	4.7	7
	(16641)	10^{-5}	5522.9	203.3	199.2	577	2.8	4
		10^{-6}	13506.2	1353.6	1325.6	3795	1.9	3
	adaptive	10^{-4}	5.2	2.9	2.9	72	3.4	5
	(≈ 2000)	10^{-5}	23.1	17.6	17.5	447	2.2	4
		10^{-6}	70.2	117.9	117.8	2968	1.5	3
0.1	0.01105	10^{-4}	1374.6	17.9	17.8	70	3.3	6
	(16641)	10^{-5}	4179.5	103.4	105.6	409	2.0	5
		10^{-6}	10111.0	793.1	727.6	2922	1.5	4
	0.00552	10^{-4}	—	130.3	134.5	91	4.3	10
	(66049)	10^{-5}	—	750.7	754.5	524	2.6	6
		10^{-6}	181285.1	4905.4	4813.2	3362	1.7	5
	adaptive	10^{-4}	45.1	5.1	5.1	69	3.3	7
	(≈ 3600)	10^{-5}	74.5	27.7	28.2	403	2.0	4
		10^{-6}	390.2	198.7	194.0	2897	1.4	3
0.05	0.00552	10^{-4}	11145.0	126.6	—	88	4.2	7
	(66049)	10^{-5}	72715.0	592.0	597.3	497	2.4	6
		10^{-6}	192554.4	3911.3	4013.2	3275	1.7	5
	adaptive	10^{-4}	737.1	13.6	—	85	4.0	7
	(≈ 7000)	10^{-5}	602.3	76.8	73.4	503	2.5	6
		10^{-6}	1478.2	467.6	478.1	3260	1.6	5

Table 1: CPU–Runtimes and iteration counts for Example 2.

discretization are nearly the same except for the failures and hence not listed. The average number of PDAS-iterations depend more on the time step than on the mesh. This is an expected behavior since when we use larger time steps the active sets change on a bigger scale than with smaller time steps. In most of the above simulations the maximum number of iterations was needed in the first time step. The reason is that the mean curvature of the interface is high in the beginning of the time evolution, resulting in fast movement of the interface region. Even taking a rather large time step, like for example $\tau = 10^{-4}$ for $\pi\varepsilon = 0.05$, the maximum number of necessary iterations per time step keeps low and never exceeded 11. The averaged numbers of iterations are much smaller since the time evolution of the interface becomes slow for larger t, resulting in only one or two PDAS-iterations.

In Figure 7 we plot the time against the number of used PDAS-iterations per time step as well as against the number of changed vertices per time step for the above simulation with $\pi\varepsilon = 0.1$, $\tau = 10^{-5}$, in the semi-implicit and implicit case for

an adaptive mesh with $h_{fine} = 0.00552$. In the first few time steps the evolution

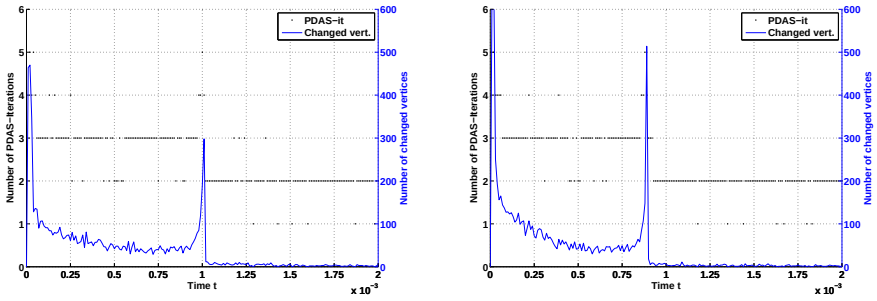

semi-implicit PDAS implicit PDAS

Figure 7: PDAS-iterations and vertices changing sets per time step.

smoothens the interfaces and the concave part is moving quickly. These two facts result in an increased number of neccessary PDAS-iterations. After that typically two to four iterations are sufficient. The steps where we only need two iterations are optimal in a way that if there is any change in the active set we need at least these two iterations. Only when there are no changes in the sets just one iteration is sufficient. What we can observe in these plots is the expected rise in iteration numbers when there is a big change in the active set. The second peak is due to the disappearance of the bubble in the upper right quadrant. If we use an equidistant mesh for the above example, the results and numbers of PDAS-iterations stay nearly the same, although in the adaptive case we have to adapt the starting active set due to a grid change in time (see 3.).

However, instead of circa 10 minutes CPU-time for an equidistant grid only 76 seconds CPU-time is needed in the adaptive case to determine a solution up to $T = 0.02$. Further speed up can be obtained as mentioned before by a different linear algebra solver.

Example 3: Random initial data

In applications one often has to consider initial data which are a random perturbation of a equally distributed concentration u. Therefore we give also results on an equally distributed mass on $\Omega = (0,1)^2$ with a stochastic distortion. As translation away from 0 we choose 0.2 and 0.7 as the range of values created and define $u_0(x) := 0.5 \cdot \sigma(x) + 0.2$, where $\sigma : \mathbb{R} \to [-1,1]$ denotes a random number generator. Consequently there is no pure phase initially, i.e. all vertices are inactive, and the resulting equation system (45)-(47) is as large as possible. For this simulation we used the implicit discretization and a uniform mesh with $h = 0.00552$, $\tau = 10^{-5}$, $T_{end} = 0.005$, $\pi\varepsilon = 0.05$ and $\mathbf{c} = 10$. In each timestep where a new active set emerges, we observe larger values in the Lagrangian multiplyier μ, namely $max\,|\mu| \approx 20$. Figure 8 shows u, w and μ after 0, 5, 50 and 500 time steps. Already after 5 time steps the phase separation can be clearly seen. In Figure 9 we see that in the early stage of this simulation one PDAS iteration is sufficient since there is

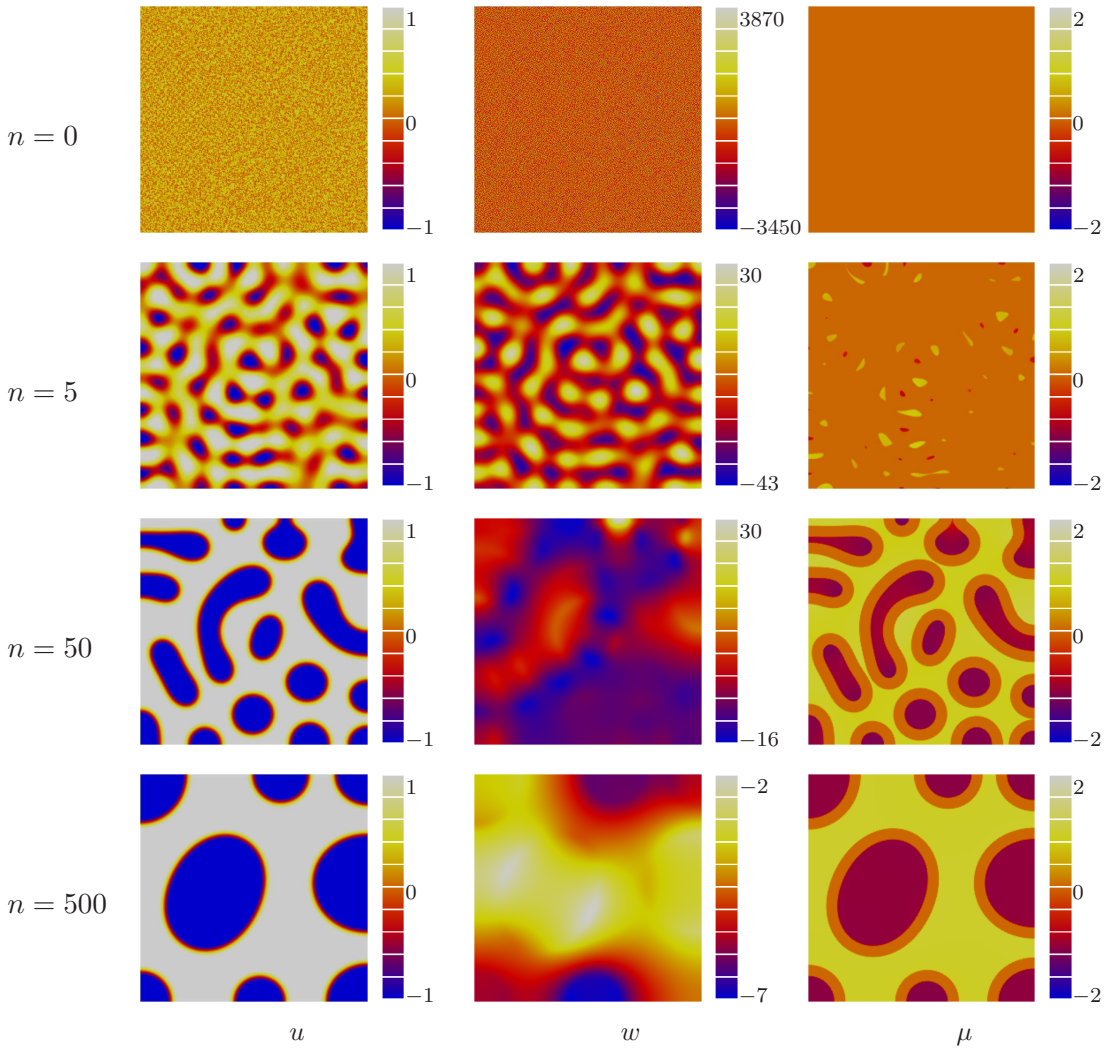

Figure 8: 2D simulation with random initial data

no active set present and we just have to solve the equation system. After that a larger number of iterations is neccessary because there are quite a few topological changes in the active set and a huge amount of vertices is changed from inactive to active. However there have never been more than 10 PDAS-iterations necessary. Afterwards when the interfaces are well developed an average amount of 2-3 iterations is sufficient.

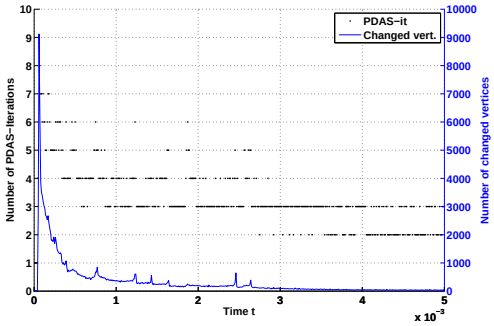

Figure 9: PDAS-iterations and vertices changing sets per time step for random initial data.

Example 4: Three dimensional simulation

Finally we give an example in 3D. Therefore we expand Example 2 to initial data consisting of four balls in $\Omega = (0,1)^3$. Figure 10 shows the 0–level sets of u of such a simulation with $\tau = 10^{-5}$, $\pi\varepsilon = 0.1$ and $\mathbf{c} = 10$ after 0, 20, 50, 100, 300 and 700 time steps on an adaptive mesh with the semi-implicit primal-dual active set solver. The simulation up to $T_{end} = 0.0007$, i.e. 70 time steps, where a coupled system

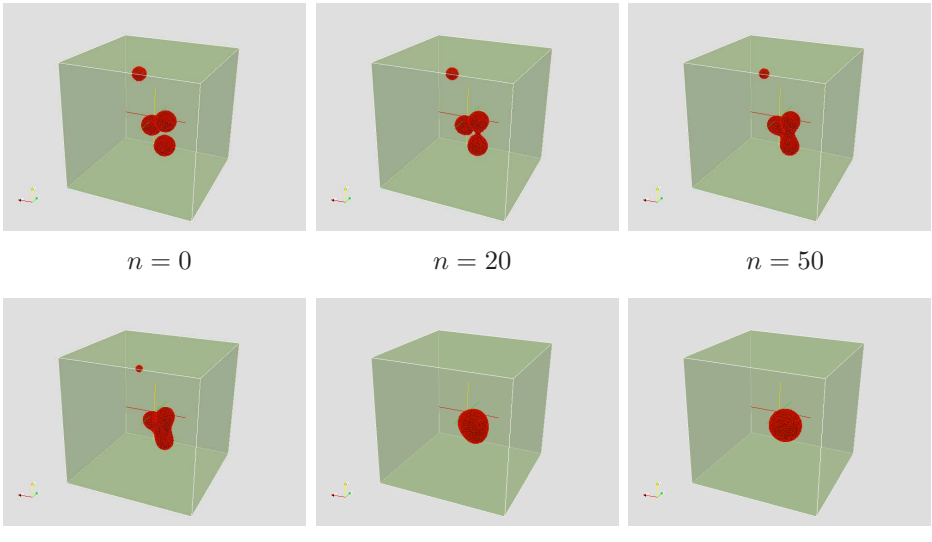

$n = 0$ $n = 20$ $n = 50$

$n = 100$ $n = 300$ $n = 700$

Figure 10: 3D simulation with 4 spheres as initial data

corresponding to roughly 120000 grid points has to be solved, took 11.8 hours with a total of 184 PDAS-iterations. This is less than half the computation time used by the pSOR method which used 27.6 hours. Additional speed up -which is not possible for the pSOR-method- can be obtained by a different LA-solver. Even for this three dimensional problem with the topological changes a maximal number of only four PDAS-iterations in each time step is sufficient for the simulation.

References

[1] Adams, R.A., *Sobolev spaces*, Pure and Applied Mathematics 65. Academic Press New York-London (1975).

[2] Banas, L. and Nürnberg, R., *On multigrid methods for the Cahn-Hilliard equation with obstacle potential*, Computational Linear Algebra with Applications, Harrachov, Czech Republic, August 19-25, 2007.

[3] Barrett, J.W., Blowey, J.F. and Garcke, H., *Finite element approximation of the Cahn–Hilliard equation with degenerate mobility*, SIAM J. Numer. Anal. 37 (1999), no. 1, 286–318.

[4] Barrett, J.W., Nürnberg, R. and Styles, V., *Finite element approximation of a void electromigration model*, SIAM J. Numer. Anal. 42 (2004), 738–772.

[5] Benzi. M., Golub., G.H. and Liesen, J., *Numerical solution of saddle point problems*, Acta Numerica (2005), 1–137.

[6] Blank, L., Garcke, H., Sarbu, L. and Styles, V., *Primal-dual active set methods for Allen-Cahn variational inequalities with non-local constraints*, Preprint SPP1253-09-01.

[7] Blowey, J.F. and Elliott, C.M., *The Cahn-Hilliard gradient theory for phase separation with nonsmooth free energy. I*, Mathematical analysis. European J. Appl. Math. 2, no.3 (1991), 233–280.

[8] Blowey, J.F. and Elliott, C.M., *The Cahn-Hilliard gradient theory for phase separation with nonsmooth free energy. II*, Numerical analysis. European J. Appl. Math. 3, no.2 (1992), 147–179.

[9] Blowey, J.F. and Elliott, C.M., *Curvature dependent phase boundary motion and parabolic double obstacle problems*, IMA Vol. Math. Appl. 47, Springer, New York (1993), 19–60.

[10] Cahn, J.W. and Hilliard, J.E., *Free energy of a nonuniform system. I*, Interfacial energy, J. Chem. Phys. 28 (1958), 258–267.

[11] Chen, X., Nashed, Z., and Qi, L., *Smoothing methods and semismooth methods for nondifferentiable operator equations*, SIAM J. Numer. Anal. 38, no.4 (2000), 1200–1216.

[12] Chen, X., *Global asymptotic limit of solutions of the Cahn–Hilliard equation*, J. Differential Geom. 44, no.2 (1996), 262–311.

[13] Davis, T.A., *Algorithm 832: UMFPACK, an unsymmetric-pattern multifrontal method*, ACM Trans. Mathematical Software, 30(2) (2003), 196–199.

[14] Davis, T.A., *A column pre-ordering strategy for the unsymmetric-pattern multifrontal method*, ACM Trans. Mathematical Software, 34(2) (2003), 165–195.

[15] Davis, T.A. and Duff, I.S., *An unsymmetric–pattern multifrontal method for sparse LU factorization*, SIAM J. Matrix Anal. Appl. 18 (1997), 140–158.

[16] Dolcetta, I.C., Vita, S.F. and March, R., *Area-preserving curve-shortening flows: From phase separation to image processing*, Interfaces and Free Boundaries 4 (4) (2002), 325–434.

[17] Duff, I.S. and Reid, J.K. *The multifrontal solution of indefinite sparse symmetric linear*, ACM Transactions on Mathematical Software (TOMS) 9 (1983), 302-325.

[18] Elliott, C.M., *The Cahn-Hilliard model for the kinetics of phase separation*, Mathematical models for phase change problems, Internat. Ser. Numer. Math. 88, Birkhäuser, Basel (1989).

[19] Evans, L.C., *Partial differential equations*, Graduate Studies in Mathematics 19. American Mathematical Society, Providence, RI (1998).

[20] Friedman, A., *Variational principles and free-boundary problems*, Wiley 1982.

[21] Garcke, H., *Mechanical effects in the Cahn-Hilliard model: A review on mathematical results*, in "Mathematical Methods and Models in phase transitions", ed.: Alain Miranvielle, Nova Science Publ. (2005), 43–77.

[22] Gräser, C. and Kornhuber, R., *On preconditioned Uzawa-type iterations for a saddle point problem with inequality constraints*, Domain decomposition methods in science and engineering XVI, 91–102, Lect. Notes Comput. Sci. Eng., 55, Springer, Berlin 2007.

[23] Hintermüller, M., Ito, K. and Kunisch, K. *The primal-dual active set strategy as a semismooth Newton method*, SIAM J. Optim. 13 (2002), no. 3, 865–888 (electronic) (2003)

[24] Ito, K. and Kunisch, K., *Semi-smooth Newton methods for variational inequalities of the first kind*, Mathematical Modelling and Numerical Analysis 37, no. 1 (2003), 41–62.

[25] Irons, B.M. *A frontal solution scheme for finite element analysis*, Int. J. Numer. Methods Eng. vol. 2 (1970), 5–32.

[26] Kinderlehrer, D. and Stampacchia, G. *An introduction to variational inequalities and their applications*, Academic Press 1980.

[27] Kuhl, E. and Schmid, D.W., *Computational modeling of mineral unmixing and growth: An application of the Cahn-Hilliard equation*, Computational Mechanics 39, no 4 (2007) pp. 4394-451 (13).

[28] Liu, J.W.H., *The multifrontal method for sparse matrix solution: Theory and practice*, SIAM Review 34 (1992), 82–109.

[29] Lowengrub, J. and Truskinovsky, L., *Quasi-incompressible Cahn-Hilliard fluids and topological transitions*, R. Soc. Lond. Proc. Ser. A Math. Phys. Eng. Sci. 454, no. 1978 (1998), 2617–2654.

[30] Novick-Cohen, A., *The Cahn-Hilliard equation: mathematical and modeling perspectives*, Adv. Math. Sci. Appl. 8, no. 2 (1998), 965–985.

[31] Ockendon, J. and Elliott, C.M., *Weak and Variational Methods for Moving Boundary Problems*, Pitman Research Notes in Mathematics, 59 (1982).

[32] Pego, R.L., *Front migration in the nonlinear Cahn–Hilliard equation*, Proc. Roy. Solc. London, Ser. A 422 (1989), 116–133.

[33] Tremaine, S., *On the origin of irregular structure in Saturn's rings*, Ast. Journal 125 (2003), 894–901.

[34] Tröltzsch, F., *Optimale Steuerung partieller Differentialgleichungen: Theorie, Verfahren und Anwendungen*, Vieweg Verlag (2005).

[35] Schmidt, A. and Siebert, K.G., *Design of adaptive finite element software: The finite element toolbox ALBERTA*, Lect. Notes Comput. Sci. Eng., 42, Springer, Berlin 2005.

[36] Stoth, B., *Convergence of the Cahn–Hilliard equation to the Mullins–Sekerka problem in spherical symmetry*, J. Diff. Eqns 125 (1996), 154–183.

[37] Zhou, S. and Wang, M.Y., *Multimaterial structural topology optimization with a generalized Cahn-Hilliard model of multiphase transition*, Structural and Multidisciplinary Optimization 33 (2007), 89–111.